Backscattering and common-base current gain of the Graphene Base Transistor (GBT)

S. Venica, F. Driussi, P. Palestri, L. Selmi
DIEGM, University of Udine and IU.NET, via delle Scienze 208, Udine 33100, Italy
E-mail address of corresponding author: venica.stefano@spes.uniud.it

Introduction: A new device based on tunneling across thin dielectrics and 2D materials has been proposed recently: the Graphene Base Transistor (GBT, [1]). It is a vertical structure where a low resistance graphene base (B, the control electrode, x=0 in **Fig. 1**) is separated from a metal or semiconducting emitter (E) and a metal collector (C) by emitter-base and base-collector insulators (EBI and BCI, respectively). In normal operation (V_{BE}>0, V_{CB}>0), electrons tunnel into the EBI conduction band (CB), cross the base perpendicularly to the graphene sheet (GR) and drift across the BCI (**Fig. 1**). The GBT functionality has been experimentally demonstrated in DC [1, 2] and simulations predict cut-off frequencies (f_T, f_{MAX}) in the THz range [3, 4]. Ideally, the graphene should be transparent to the electrons' flow; in practice, experiments show a large base current (I_B) that severely limits the common-base current gain (α_F=I_C/I_E) [1, 2].

Abstract: *In this paper, we investigate electron transport and backscattering in the EBI and BCI as possible root causes of the base current and of the common-base current gain degradation in GBTs by means of a Monte Carlo (MC) transport model. Backscattering limited α_F values are found to be much higher than experiments in [1, 2], suggesting that state-of-the-art technology is still far from being optimized, but they are low enough to limit the maximum achievable performance.*

Model: To study α_F in the GBT, we developed a dedicated single-particle Monte Carlo simulator for transport in EBI and BCI. Consistently with [4], we neglect hole injection from the GR to the EBI, since it is expected to provide a negligible reduction of the emitter efficiency, hence of α_F. We extend the model of [5] to a non-parabolic CB with non-parabolicity parameter α (**Tab. 1**). Both emission and absorption of polar optical and non-polar acoustic phonons in the dielectrics are considered as scattering mechanisms. We assume injection into the EBI CB (at x_{inj}, **Fig. 1**) by Fowler-Nordheim tunneling from the emitter Fermi energy. Electron free flights and scattering events are alternated until particles exit the GBT, either arriving from the BCI with positive velocity to the C terminal (contributing to I_C), or impinging the GR with negative velocity due to backscattering in the BCI (contributing to I_B, **Fig. 1**). Then we calculate $\alpha_F = I_C/(I_C+I_B)$. In the lack of a consolidated theoretical framework to compute the direct capture by the GR of electrons impinging the EBI/GR interface, this contribution to I_B is neglected. Calculated α_F is thus an upper estimate. We start with SiO_2 EBI and BCI, since calibrated scattering parameters are available ([6], **Tab. 1**), and then we analyze high-*k* EBI and BCI as used in optimized GBTs [3, 4].

Results: **Fig. 2** shows the electron concentration (n) and average velocity (v_x) for a few V_{BE} values. The abscissa x_{inj} moves backward as V_{BE} is increased, as expected. The n in the EBI decreases along x (**Fig. 2a**), because electrons are accelerated by the field (**Fig. 2b**). In the BCI, instead, n and v_x are essentially constant. This result confirms the assumptions behind the electrical model in [3] that estimates the maximum f_T by accounting for space charge effects.

Fig. 3a shows the average kinetic energy (AKE) of electrons at the EBI/GR interface computed with and without scattering. Scattering induces a limited energy relaxation in the EBI layer. **Fig. 3b** reports the probability density of the angle (θ, inset in **Fig. 1**) between the electron velocity and the x axis for the electrons hitting the EBI/GR interface from the left; the distribution peak approaches θ=0 as V_{BE} increases, due to preferential orientation of the velocity vector. Concerning the transport in the BCI, for increasing V_{BE}, the AKE of electrons entering the BCI is larger (**Fig. 3a**), hence, the average number of backscatterings in the BCI increases, I_B increases and α_F is reduced (**Fig. 4**). Therefore backscattering sets an upper limit to α_F. In addition, the field in the BCI decreases for increasing BCI thickness, leading to more backscatterings and reduced α_F (**Fig. 4b**). A similar trend is observed for increasing EBI thickness (**Fig. 4a**). Optimized GBTs typically feature different materials for the EBI and BCI [3, 4]. For $\Delta E=(\chi_{BCI}-\chi_{EBI})>0$ (see **Fig.1**, where χ is the electron affinity) the AKE in the BCI and the fraction of electrons that suffer backscattering increase, further reducing α_F (empty symbols, **Fig. 4a**). For comparison with available data [1], we also simulated a GBT with a 5.0 nm SiO_2 EBI and a 25 nm Al_2O_3 BCI. Scattering parameters are those in **Tab. 1**, where the Al_2O_3 acoustic phonon scattering deformation potential C_{ae} is tentatively set equal to that of SiO_2. The simulated α_F (**Fig. 5)** shows V_{BE} and V_{CB} dependencies consistent with experiments of [1] (not shown), while the calculated values (0.5-0.9) are much larger than measurements (10^{-3}-7×10^{-2}) [1, 2], but still small enough to pose a severe limit to the GBT static performance. If the scattering probability in the BCI is increased by choosing C_{ae} as high as 10 eV, α_F decreases (triangles vs. circles in **Fig. 6a**), but not enough to match the measurements. Moreover, the V_{BE} dependence becomes stronger, while the V_{CB} dependence is reduced (**Fig. 6b**). An increase of the CB mass up to $0.6m_0$ (possibly justified by the large electron-phonon coupling in Al_2O_3 [7, 8]) lowers α_F, but again not enough to match the experiments (**Fig. 7**).

Conclusions: the results of the MC simulations validate some of the assumptions made to develop the GBT performance model in [3], and suggest that backscattering from the BCI to the GR can pose a severe limit to α_F. The parameter uncertainties appear inadequate to reconcile simulations with experiments, thus pointing out that additional physical mechanisms (e.g. interface traps and direct electron capture by the GR) are responsible for the low measured α_F and further device optimization is needed.

Acknowledgments: This research activity has received funding by the UE through the STREP project GRADE (317839). The authors acknowledge D. Esseni (University of Udine), S. Vaziri (KTH) and M. C. Lemme (University of Siegen) for fruitful discussions.

[1] S. Vaziri et al., *NanoLetters* 13 (2013), 1435-1439
[2] C. Zeng et al., *NanoLetters* 13 (2013), 2379-2375
[3] S. Venica et al., *IEEE TED* 61 (2014), *2570*
[4] V. Di Lecce et al., *IEEE TED* 60 (2013), 3584
[5] M. V. Fischetti et al., *Phys. Rev. B* 31 (1985), 8124
[6] P. Palestri et al., *Proc. of SISPAD 2000*, 38
[7] V. G. Kravets, *Phys. Rev. B* 72 (2005), 064303
[8] J. Shan et al., *Phys. Rev. Lett.* 90 (2003), 247401
[9] S. Spiga et al., *Appl. Phys. Expr.* 5 (2012), 021102
[10] M. V. Fischetti et al., *J. Appl. Phys.* 90 (2001), 4587

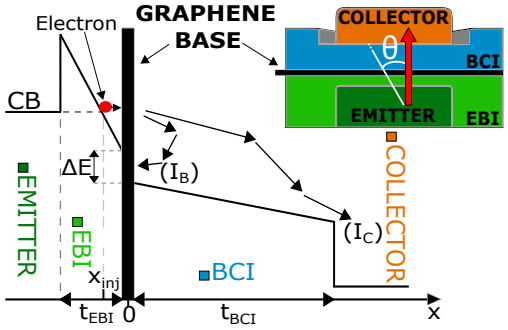

***Fig. 1**: Conduction band diagram of the GBT. The electrons injected from the EBI through the graphene scatter in the BCI and either reach the collector (contributing to I_C) or backscatter to the base and captured by the graphene (thus contributing to I_B). The inset shows the GBT structure and the definition of θ.*

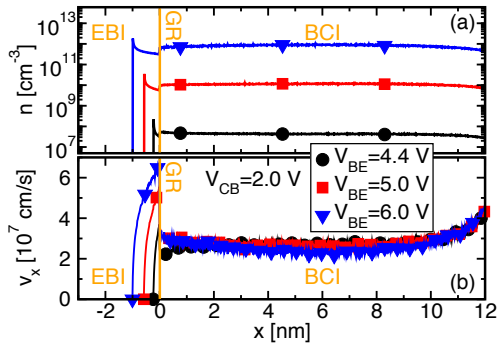

***Fig. 2**: Electron concentration (top) and average electron velocity (bottom) along a GBT device with EBI and BCI made in SiO_2 (t_{EBI}=3nm, t_{BCI}=12 nm) for a few values of V_{BE}.*

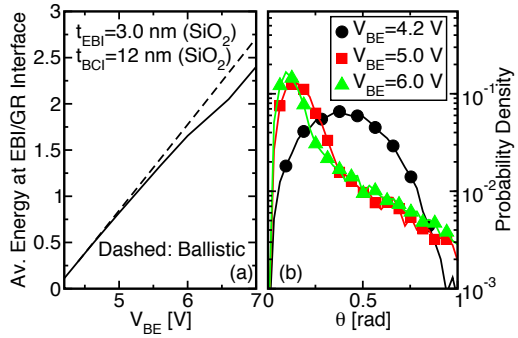

***Fig. 3**: Electron energy (a) and probability distribution of the angle θ (inset in Fig. 1) of incidence (b) at the EBI/GR interface (x=0 in Fig. 1). Ballistic electron transport is reported as a reference (dashed line).*

Units	χ eV	m_I m_0	α eV^{-1}	ε_{stat} ε_0	ε_{int} ε_0	ε_∞ ε_0	ω_{LO1} meV	ω_{LO2} meV	C_{ae} eV
SiO_2	0.95	0.5	0.2	3.9	3.15	2.19	153	63	2.1
Al_2O_3	1.65 [9]	0.4 [9]	0.2	10 [9]	7.27 [10]	3.2 [10]	109 [8]	63.3 [8]	2.1

***Tab1**: Scattering parameters used in the simulations of Fig. 5. SiO_2 parameters from [6].*

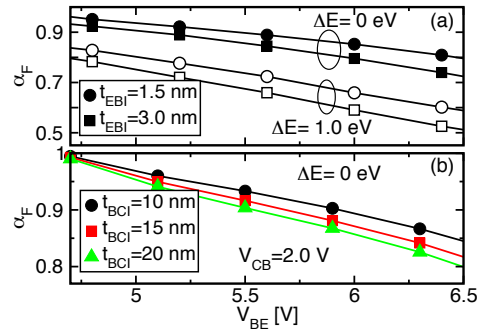

***Fig. 4**: α_F versus V_{BE} for different EBI thickness (t_{EBI}) and ΔE for t_{BCI}=12 nm (a) and for different BCI thickness (t_{BCI}) with t_{EBI}=2 nm (b). EBI and BCI made of SiO_2.*

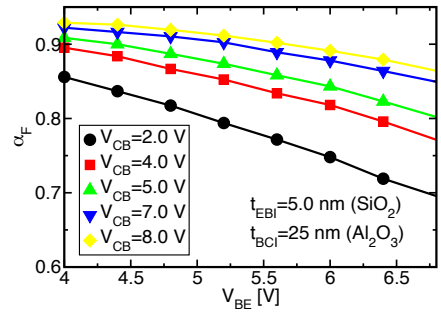

***Fig. 5**: Simulated α_F as a function of V_{BE} for a GBT with EBI in SiO_2 and BCI in Al_2O_3. Scattering parameters as in Tab.1.*

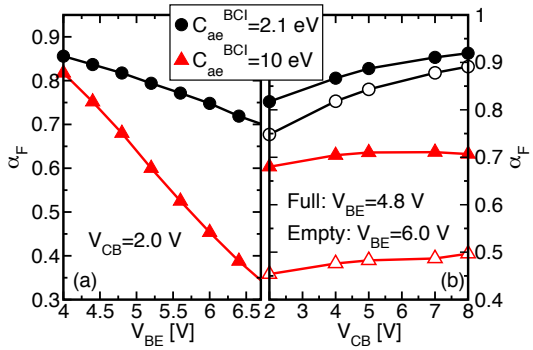

***Fig. 6**: Simulated α_F as a function of V_{BE} (a) and V_{CB} (b) for the GBT of Fig. 5. C_{ae} is used as a free parameter.*

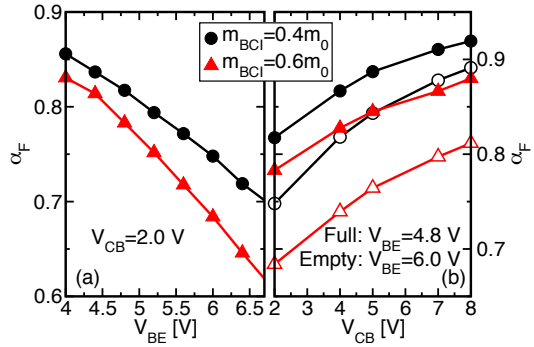

***Fig. 7**: Simulated α_F as a function of V_{BE} (a) and V_{CB} (b) for the GBT of Fig. 5 and by using m_I as a parameter.*